The 14th International Topical Meeting on Nuclear Reactor Thermalhydraulics, NURETH-14
Toronto, Ontario, Canada, September 25-30, 2011

NURETH14-229

VIPRE-W / MEFISTO-T – A MECHANISTIC TOOL FOR TRANSIENT PREDICTION OF DRYOUT IN BWR FUEL

Carl Adamsson[1,2] and Jean-Marie Le Corre[1]
[1] Westingouse Electric Sweden, Västerås, Sweden.
[2] currently at Paul Scherrer Institut, Villigen, Switzerland
carl.adamsson@psi.ch ; lecorrjm@westinghouse.com

Abstract

The VIPRE-W/MEFISTO-T code package constitutes a simplified approach to sub-channel film-flow analysis whereby the transport equations for the liquid films are decoupled from each other. The approach allows fast and robust simulation with high axial resolution of realistic BWR transients. It has previously been shown that a steady-state version of the model agrees well with dryout measurements in full-scale fuel assembly mock-ups performed at the Westinghouse FRIGG loop. In this paper, we present validation of the transient version of the code with around 300 transient dryout experiments from the same loop. The transients involve realistic variations of flow and power and three different axial power distributions at conditions typical for BWR operation. The results from the film-flow analysis show high precision in the dryout prediction but a hitherto unexplained bias that reduces the accuracy.

1. Introduction

Safety analysis for boiling water reactors (BWR) is typically performed with one-dimensional system codes equipped with purely empirical dryout correlations to predict the thermal margins. Three-dimensional effects, such as the influence of the internal power distribution, must be implicitly handled by the dryout correlation. Considering that these effects develop over a length scale that is comparable to the height of a typical fuel assembly it is questionable if they can be incorporated in a simple algebraic correlation [1]. This is the reason why several three-field subchannel codes for BWR thermal hydraulics have been developed, e.g. the COBRA-TF code [2], the NASCA code [3] and the FIDAS code [4]. The MONA-3 code [5] may also be classified as a three- field code even though some of the momentum and energy equations have been lumped. The development of these models is an ongoing effort with the main focus to improve accuracy and to bring the empirical parts of the models closer to the underlying physics. A recent contribution in this direction is the work by Lane et al. [6].

Three-field two-phase thermal hydraulics differs conceptually from the more commonly used two-phase (two or one-field) models in several ways. They eliminate the need for empirical correlations for phase-slip, two-phase multipliers and the critical heat flux. Instead more mechanistic concepts such as interfacial friction factors and various lateral mass-transfer mechanisms are introduced. The mechanistic concepts are believed to be more generally applicable and to capture phenomena that might be overlooked by the simpler empirical formulations. On the other hand, it is difficult to obtain the detailed experimental data that is often necessary for the direct validation of such models and the complexity of the models can make the codes impractical for engineering applications. For

this reason, we believe that mechanistic models should be used when they are necessary in order to describe relevant an important physical phenomena but when there is no such clear advantage one should consider simpler models that are easier to validate.

The present work is an extension of a previously presented and extensively validated model [7] in order to include transient applications. It pursues an intermediate path between a full three-field formulation and most common two-phase flow models. The technique is based on the decoupling of the film equations so that they can be solved as a post-process, relying on a standard two-phase flow approach. Our main goal is not the elimination of all empirical models and correlations. Instead we want to eliminate complexity and use additional equations only when similar capabilities could clearly not have been achieved with a simpler model. The intention is not to create a general purpose thermal-hydraulic model. Instead we focus strictly on the modelling of the high-quality dryout phenomenon as it appears in boiling water reactors.

2. Basic equations

In this section we present the fundamental conservation equations, which form the basis of the film model. In the steady-state limit they reduce to the equations used in [7]. In that case, however, the momentum equation (section 2.3) decouples from the model and it can be excluded.

The typical modelling approach and equations used in standard two-phase subchannel codes are described in [8]. Complete three-field formulations have been published by Sugawara [9] and Jayanti and Valette [10]. A slightly simplified three-field alternative was described by Hoyer [11]. Based on the three-field formulations we present here a simplified set of equations for the liquid film in annular two-phase flow. Terms that are of minor importance in the annular flow regime have been removed from the equations. Further simplification of the energy and momentum equations is achieved by introducing a few equilibrium assumptions that are motivated by the length and time scales that prevail in a typical BWR nuclear fuel assembly. The equations are presented here for a single liquid film in order to simplify the notation. In the actual implementation we allow any number of films in each subchannel. We assume that two-phase (mass and enthalpy) solution is available from the driver code when the film-equations are solved.

2.1 Mass equation

Selecting a control volume that contains the liquid film to be analyzed and assuming a single film thickness, δ, throughout this control volume and an average film velocity, u_f, we arrive at the following mass-balance equation:

$$\frac{\partial}{\partial t}\left(\Pi\rho_l\delta\right)+\frac{\partial}{\partial z}\left(u_f\Pi\rho_l\delta\right)=\Pi\left(D-E-\Gamma\right)+w_f \tag{1}$$

where Π is the wall perimeter, ρ_l is the liquid density, D, E and Γ denote the rate of deposition, entrainment and evaporation, respectively and w_f is the cross-flow of liquid film into the control volume per unit axial distance (see section 3.4). We have the following relation between the film flow-rate, W_f, the film thickness and film velocity:

$$W_f = u_f \Pi \rho_l \delta , \tag{2}$$

which may be considered the definition of the film thickness. Inserting (2) into equation (1) gives:

$$\frac{\partial}{\partial t}\left(\frac{W_f}{u_f}\right) + \frac{\partial}{\partial z}\left(W_f\right) = \Pi\left(D - E - \Gamma\right) + w_f \tag{3}$$

Equations (1) and (3) are equivalent; the only difference is whether δ or W_f is considered as a primitive variable. We prefer the latter form because it decouples the mass-equation from the momentum equation in the steady-state limit.

2.2 Energy equation

By considering the same control volume as in section 2.1 the following equation for the energy balance is obtained:

$$\frac{\partial}{\partial t}\left(h_f \frac{W_f}{u_f}\right) + \frac{\partial}{\partial z}\left(h_f W_f\right) = \Pi\left(D h_d - E h_d - \Gamma h_g + q''\right) + w_f h_f , \tag{4}$$

where q'' is the wall heat flux, h denotes enthalpy and *f*, *d* and *g* refer to the film, drop and gas fields, respectively. This equation may be simplified by assuming thermal equilibrium, i.e. that the temperature of both phases are always equal to the saturation temperature, which is a good approximation for the annular flow regime. This assumption is equivalent to setting $h_f = h_d = h_{ls}$ and $h_g = h_{gs}$. Substituting this and subtracting equation (3) times h_{ls} gives:

$$\left(\frac{\partial h_{ls}}{\partial t} + u_f \frac{\partial h_{ls}}{\partial z}\right)\rho_l \delta = -\Gamma h_{gs} + \Gamma_{ls} + q'' \tag{5}$$

and introducing the pressure, p,

$$\left(\frac{\partial p}{\partial t} + u_f \frac{\partial p}{\partial z}\right)\rho_l \frac{\partial h_{ls}}{\partial p}\delta = -\Gamma h_{gs} + \Gamma_{ls} + q'' \tag{6}$$

For pressure between 20 and 200 bar $\rho_l \partial h_{ls} / \partial p < 100$. Setting the pressure rate of change to 10 bar/s and the film thickness to 0.1 mm the left hand side is equivalent to a heat flux of less than 10 kW/m^2, which is negligible compared to the typical surface heat flux of a nuclear fuel rod. Neglecting the left hand side we get:

$$\Gamma = \frac{q''}{h_{gs} - h_{ls}} = \frac{q''}{h_{\mathrm{lg}}} \tag{7}$$

This simplification of a partial differential equation into an algebraic relation has been achieved primarily by assuming thermal equilibrium between the phases and by neglecting secondary heat sources such as frictional heating and phase change related to change in pressure. It may be noted

that (7) does not include any time-dependent terms and hence is identical to the energy equation of the steady-state model.

2.3 Momentum equation

Again considering the same control volume as in section 2.1 and assuming that droplets are deposited with the average droplet velocity, u_d, and entrained with the film velocity, u_f, we get:

$$\frac{\partial}{\partial t}W_f + \frac{\partial}{\partial z}\left(u_f W_f\right) = \Pi\left(u_d D - u_f E - u_f \Gamma\right) + u_f w_f - \Pi\delta\left(\frac{\partial p}{\partial z} + g\rho_l\right) + \Pi\left(\tau_i - \tau_w\right) \tag{8}$$

where τ_i and τ_w denote the shear stresses at the film interface and at the wall, respectively and g is the acceleration of gravity. Multiplying equation (3) with u_f and subtracting from equation (10) this can, by using equation (2), be rearranged into:

$$\left(\frac{1}{u_f}\frac{\partial u_f}{\partial t} + \frac{\partial u_f}{\partial z}\right)\rho_l \delta \Pi u_f = \Pi D\left(u_d - u_f\right) - \Pi\delta\left(\frac{\partial p}{\partial z} + g\rho_l\right) + \Pi\left(\tau_i - \tau_w\right) \tag{9}$$

Because the film is very thin the contribution from the pressure gradient, gravity and inertia terms are negligible. The momentum transfer by deposition can, however, be considerable and should not be neglected [12]. Introducing these assumptions we have:

$$D\left(u_d - u_f\right) + \tau_i - \tau_w = 0 \tag{10}$$

and have thus reduced the momentum equation from a partial differential equation to an algebraic equation. This has been achieved by neglecting the inertia and the weight/buoyancy of the liquid film, which is motivated as long as the film is thin.

We could now proceed to introduce models for the shear stresses and the droplet velocity and solve for the film velocity. The result would be an algebraic equation for the film velocity, which provides the coupling to the mass-equation. However, the two-phase driver code already solves another momentum equation and applies a void correlation. In order to be consistent with the driver code we assume that the wall shear stress, τ_w, as calculated by the driver code is correct and related to the film velocity according to

$$\tau_w = \frac{1}{2} C_w \rho_l u_f^2, \tag{11}$$

where C_w is the wall-to-film friction factor that we model according to Wallis [13] as

$$C_w = \max\left(\frac{16}{\mathrm{Re}_f}, 0.005\right), \tag{12}$$

where Re_f is the film Reynolds number. We get the following algebraic equation for the film velocity

$$u_f = \sqrt{\frac{2\tau_w}{C_w \rho_l}}. \tag{13}$$

The momentum equation (10) has not been used explicitly; in the present approach it serves only as a motivation to use a simple algebraic expression for the film velocity rather than a differential equation.

3. Constitutive relations

3.1 Deposition

We use the formulation by Okawa et al. [14], which is a slightly modified variant of the model proposed by Hewitt and Govan [15]. Explicitly:

$$\frac{D}{C} = 0.0632\left(\frac{C}{\rho_g}\right)^{-0.5}\sqrt{\frac{\sigma}{\rho_g d_h}} \tag{14}$$

where

$$C \equiv \frac{W_d}{W_d/\rho_l + W_g/\rho_g}. \tag{15}$$

3.2 Entrainment

The entrainment correlation presented by Okawa et al. [14] is used with modifications according to [1].

$$E = k_E \rho_l \frac{C_i G_g^2 \delta_E}{\sigma \rho_g}. \tag{16}$$

Here C_i is an interfacial friction factor and δ_E is an estimate of film thickness. It is, however, not the same as the δ as defined by equation (2) but the one estimate used by Okawa et al. [14] in developing the correlation, given by

$$\delta_E = \sqrt{\frac{C_w \rho_g}{C_i \rho_l}}\frac{W_f}{\Pi}\frac{1}{G_g}. \tag{17}$$

The interfacial friction factor is given by

$$C_i = 0.05\left[1 + \frac{75}{A}\left(1 - \sum \delta\Pi\right)\right]. \tag{18}$$

where the sum goes over all walls in the subchannel. Again this is consistent with the original work by Okawa et al. but generalized to accommodate subchannels with more than one wall. Other generalizations are conceivable but we believe that there should be only a single interfacial friction factor for the entire subchannel, not a local one for each wall. The application of entrainment correlations, which were developed for pipes, to multi-wall subchannels has been discussed in more detail in [16].

3.3 Spacer grids

Spacer grids are known to have a significant and usually positive influence on the dryout margins. This is usually attributed to an increased deposition rate downstream the grid as a result of increased turbulence. We model this by multiplying the deposition rate downstream the spacer grids by a factor $k_{enh}(z,\theta)$, which is a function of the spacer blockage ratio θ and the distance, z, to the closest upstream spacer. The model has been adopted directly from the steady-state version of the code [7].

3.4 Cross-flows

Most two-phase subchannel codes and, in particular, the VIPRE-W code used in this paper model two types of lateral transport mechanisms, usually referred to as diversion cross-flows and turbulent mixing, respectively [8]. The diversion cross-flow is a net mass-flow, w_{div}, from one subchannel to a neighbor subchannel driven by a lateral pressure gradient. In VIPRE and most similar codes it is assumed that the enthalpy carried with the diversion cross-flow is the mixture enthalpy of the donor (i.e. upstream) subchannel, h_{don}.

The turbulent mixing, on the other hand, may be modeled in various ways. In single-phase flow it would typically correspond to the transport of heat from one subchannel to a neighbor without net mass-transport by heat conduction and by random turbulent motions of the fluid. This concept has been carried over to the VIPRE-W model [17] even though it is not obvious that the mass-transport should be zero when a net density gradient is present as in two-phase flows. This issue is further discussed by Lahey and Moody [8]. For the purposes of this text it suffices to note that the VIPRE-W model is empirical and that it is mainly motivated by its agreement with experiments [18]. The VIPRE-W model for turbulent mixing thus assumes no mass-transfer (in addition to the diversion cross-flow) but a net transport of enthalpy equal to $w_{TM}\Delta h$, where w_{TM} is a virtual mass-exchange rate per unit axial length and Δh is the difference in mixture enthalpies between the two neighbor subchannels.

A three-field model that does not use enthalpy as a primitive variable cannot directly adopt a cross-flow model as described above. Instead all lateral transport must be modeled as net mass-flows, w_g, w_d and w_f, of the film, droplets and gas fields. In the present case we obtain these mass-flow terms implicitly, demanding consistency with the model of the driver code in terms of mass and enthalpy. That is, we require that

$$w_{div} = w_v + w_l \tag{19}$$

$$w_{div}h_{don} + w_{TM}\Delta h = w_g h_g + w_l h_l \tag{20}$$

The liquid cross-flow, $w_l \equiv w_f + w_d$, must be further divided into a film cross-flow, w_f and a droplet cross-flow, w_d. This information cannot be derived from the two-phase driver solution. Instead we divide the cross-flow according to the proportion of film and drops in the main flow of the subchannel, i.e.

$$w_f = w_l \frac{W_f}{W_f + W_d} \tag{21}$$

where all fields refer to the same subchannel. This model is directly adopted from the steady-state model [7]. It has the advantage to decouple the film flows of the individual subchannels so that all subchannels can be analyzed independently once the two-phase solution has been obtained. It has previously been shown [7] that the model is not particularly sensitive to the details of this assumption.

4. Flow-regime transitions

The film-flow model of MEFISTO-T is valid for the annular flow-regime only. The steady-state version of the model [7] was hence applied only to the part of the channel where the flow regime is annular and the upstream boundary condition was defined at the location of onset of annular flow. For transients, however, this location will move as the transient progresses at a velocity, which may exceed the velocity, u_f, of the liquid film. In that case, defining the boundary condition at the location of onset of annular flow will result in an ill-posed set of equations. We have addressed this problem by creating a simplified model of the flow-regimes with less steam content than the annular, here collectively referred to as pre-annular flow. The only purpose of this model is to give a robust solution for the drop- and film-fields that approaches hydrodynamic equilibrium at the point of transition to annular flow in order to be consistent with the steady-state model. In pre-annular region, the droplets and film have been assigned the same velocity, which is reasonable since it is not possible to distinguish between droplets and film in these flow regimes. In order to be consistent with the solution from the driver code it is then necessary that

$$u_f = u_d = \frac{W_f + W_d}{(1-\alpha)\rho_l A}, \tag{22}$$

where α is the void fraction as calculated by the driver code. With this assumption the separation of the liquid phase into droplets and film should be quite arbitrary in the pre-annular region. However, at the transition point we want these fields to be as close to equilibrium as possible. This is achieved by estimating the equilibrium droplet fraction at the transition point and introducing the corresponding mass-flow of droplets already at the channel inlet.

The onset of annular flow is determined from the criterion by Wallis [13], which may be rearranged into an explicit equation for the transition steam quality

$$x_{tr} = \left(0.6 + 0.4 \frac{\sqrt{g d_h (\rho_l - \rho_g)\rho_l}}{G} \right) \Big/ \left(0.6 + \sqrt{\rho_l / \rho_g} \right) \tag{23}$$

where $G = W / A$ is the average total mass flux in the subchannel. We define the pre-annular flow regime to be any part of the flow where $x < x_{tr}$. Ideally none of the constitutive relations that are valid only for annular flow should be applied here. However, the model (23) must be considered as approximate. In fact, the very concept of a flow regime transition is an idealization. It thus makes sense to phase in deposition and entrainment models gradually as the transition point is approached.

This has the numerical advantage of avoiding a discontinuity in the model and, more importantly, the deposition and entrainment rates will start to approach the desired equilibrium already within the pre-annular region.

5. Validation

5.1 Transient dryout measurements in pipe

As a first step the model was validated in simple tube geometry, thereby excluding the relatively uncertain cross-flow and spacer models and staying close to the geometry for which most of the empirical constitutive relations have been developed. The results of this validation effort were presented in [19] based on an early prototype of the model described in this paper and transient measurements by Moxon and Edwards [20]. Even though the models are not identical in all details, the present model yields very similar results.

5.2 Transient dryout measurements in rod bundles

The main validation of the models is the comparison against the dryout measurements from Westinghouse FRIGG loop, performed in full-scale, realistic 24-rod quarter bundles including spacer grids and part-length rods. The validation over the steady-state database (1364 data points) has been presented in [7]. In this paper we present the validation against the transient dryout measurements from the same loop and in the same geometry using the same model parameters and discretization with 35 subchannels and 100 axial nodes. The experiments were performed with three different axial power distributions: top-peaked, cosine and bottom-peaked. Various flow-decrease and power-increase transients were included as well as combinations thereof. A total of 294 transient measurements were performed, all of which are included in the present validation.

In a transient it is not meaningful to speak about ‘critical power’, which is the main validation parameter in steady-state. The direct outcome of the transient measurements is instead the rod temperature, which could be directly validated. The present model does, however, not include post-dryout heat transfer model. The only result of the simulation is the minimum film flowrate (MFF), which acts as a measure of dryout margin. In the same way as in the steady-state case we let the film-flow rate decrease to artificial negative values if the film dries out. These negative film flows are to be interpreted as negative margin to dryout, not to correspond to any measurable quantity. For each transient we hence restrict the validation to a dryout/non-dryout comparison. This information is extracted from the experiments by inspecting the temperature traces from the thermocouples, as illustrated in Figure 1.

The validation results are summarized in Figure 2, Figure 3 and Figure 4. These figures show the maximum measured rod temperature increase versus the simulated film flowrate and indicates for each point whether or not dryout occurred during the test. The temperature increase is not formally a part of the validation but was included in order to enhance the readability of the plots. In the simulations, a dryout prediction should ideally correspond to MFF<0. We do, however, observe a systematic bias of the simulated MFF so that the onset of dryout is typically observered for MFF between 0.1 and 0.15 kg/s/m. As for now we do not have a definitive explanation for this bias. Model deficiencies cannot be ruled out but extensive sensitivity studies indicate that part or all of the

bias may be explained by the choice of various models and numerical parameters in the VIPRE-W code. On the other hand, the MFF interval where the onset of dryout occurs is rather small and it has been shown [21] that it is consistent with the standard deviation of the steady-state model.

Further validation of the model against the full-bundle transient dryout tests that were included in the BFBT benchmark [22] is presented in [23].

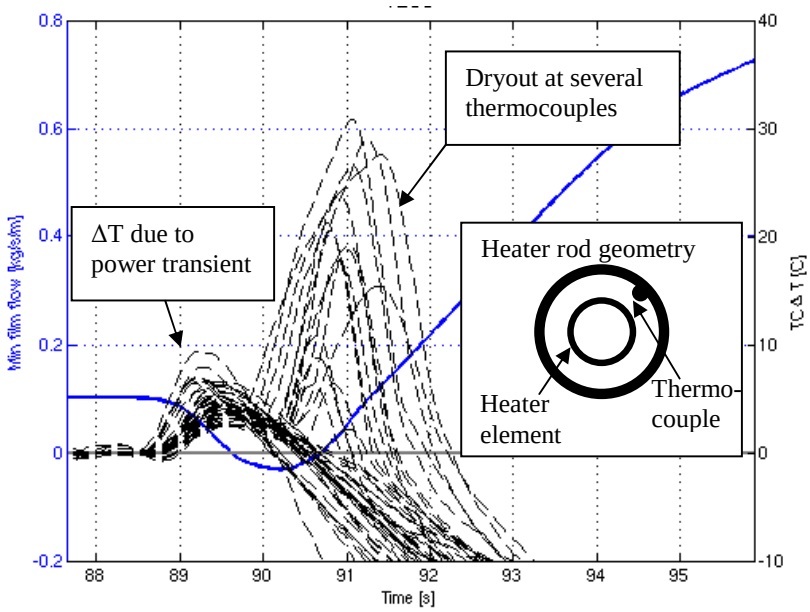

Figure 1 Example of measured temperature increase above the steady-state value (black) and simulated film-flow versus time (blue). The sudden rise of temperature at several positions indicates that dryout has occurred. The smaller temperature rise that occurs earlier and simultaneously at all positions is caused by the imposed power transient and thermocouples being located inside the heater rods rather than at the surface.

6. Conclusions

We have shown that a simplified three-field subchannel model, based on a standard two-phase subchannel code extended with a multi-wall film model, is able to reliably predict transient dryout margins in a BWR fuel assembly. A database of 294 transient dryout measurements in full-scale mock-up bundles from the Westinghouse FRIGG loop has been used as well as measurements in simple pipe geometry. Conditions are typical for BWR anticipated operational occurrences, such as load rejections and pump trips, except that experiments with fast pressure increase are not available. The model has previously been demonstrated to predict the steady-state dryout power with a standard deviation of 4.1%.[7] The transients results show that precision in the predictions is comparable to the steady-state model [21]. There is, however, a clear bias in the simulated film flow-rates that reduces the accuracy. The steady-state validation showed that the model was essentially unbiased (MFF=0 at dryout on average). It is currently not clear why this property does not apply to the transient case but there are indications that details in the subchannel model may have caused the bias.

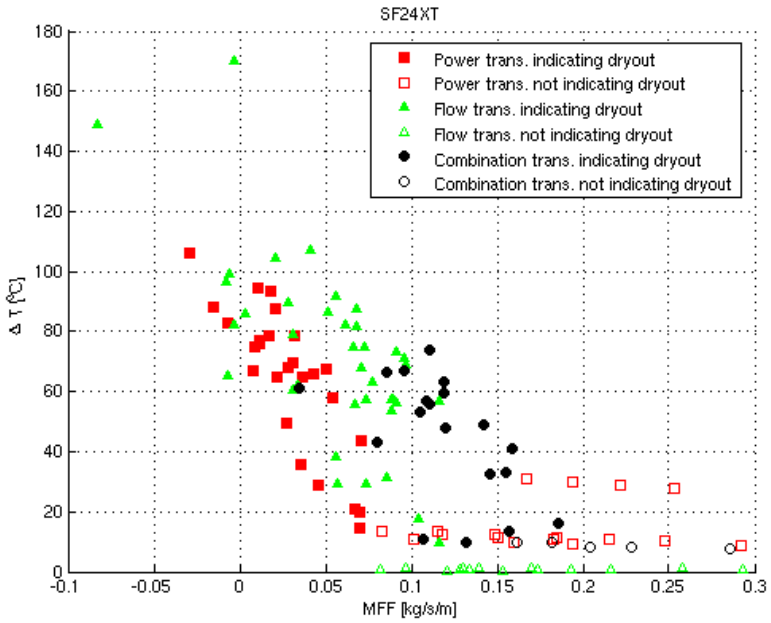

Figure 2 All experiments with top-peaked axial power distribution. Measured rod temperature increase versus simulated minimum film flowrate per unit rod perimeter (MFF).

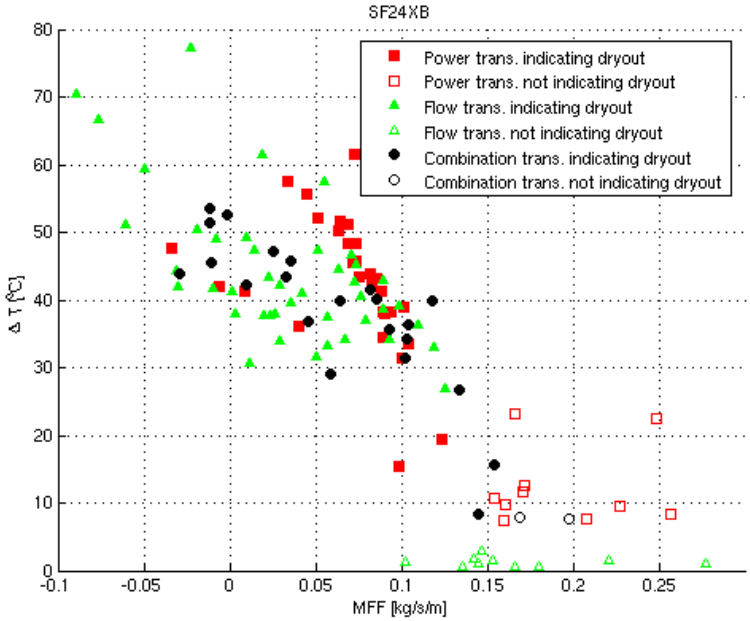

Figure 3 All experiments with cosine axial power distribution. Measured temperature versus simulated minimum film flowrate per unit rod perimeter (MFF).

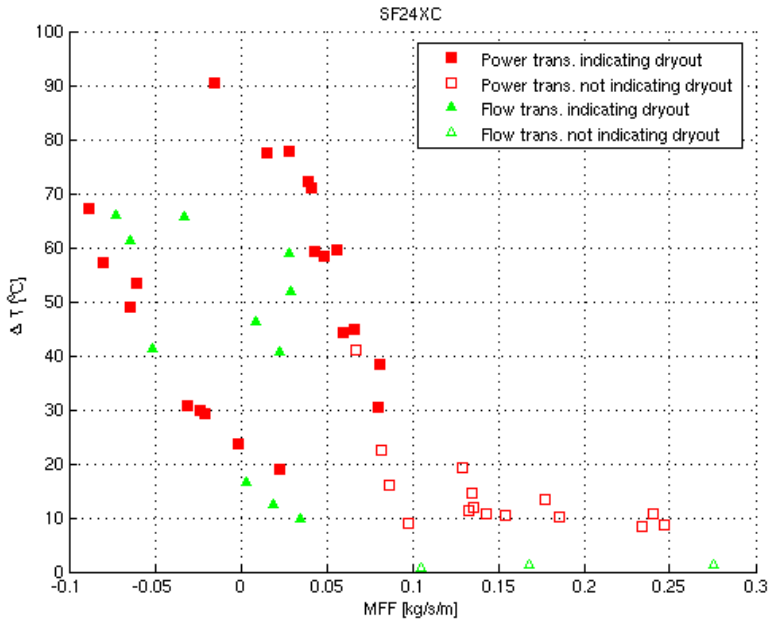

Figure 4 All experiments with bottom-peaked axial power distribution. Measured temperature increase versus simulated minimum film flowrate per unit rod perimeter (MFF).

7. References

[1] C. Adamsson and H. Anglart, "Influence of axial power distribution on dryout: Film-flow models and experiments," *Nuclear Engineering and Design*, vol. 240, no. 6, pp. 1495-1505, Jun. 2010.

[2] M. Glück, "Sub-channel analysis with F-COBRA-TF - Code validation and approaches to CHF prediction," *Nuclear Engineering and Design*, vol. 237, no. 6, pp. 655-667, Mar. 2007.

[3] H. Chitose, H. Akitoshi, O. Akir, and F. Ken, *Improvement of Predictive Accuracy on Subchannel Analysis Code (NASCA) for Tight-Lattice Rod Bundle Tests - Optimization of UEDA'S Entrainment Model Parameter and Cross Flow Model Parameters*. 2006.

[4] S. Sugawara and Y. Miyamoto, "FIDAS: Detailed subchannel analysis code based on the three-fluid and three-field model," *Nuclear Engineering and Design*, vol. 120, no. 2-3, pp. 147-161, Jun. 1990.

[5] M. Nordsveen, N. Hoyer, H. Anglart, and C. Adamsson, "The MONA Subchannel Analysis Code – Part A: Model Description," in *The 10th International Topical Meeting on Nuclear Reactor Thermal Hydraulics (NURETH-10)*, 2003.

[6] J. W. Lane, D. L. Aumiller Jr, F.-B. Cheung, and L. E. Hochreiter, "A self-consistent three-field constitutive model set for predicting co-current annular flow," *Nuclear Engineering and Design*, vol. 240, no. 10, pp. 3294-3308, Oktober. 2010.

[7] C. Adamsson and J.-M. Le Corre, "Modeling and validation of a mechanistic tool (MEFISTO) for the prediction of critical power in BWR fuel assemblies," *Nuclear Engineering and Design*, 2011 in press (doi:10.1016/j.nucengdes.2011.01.033).

[8] A. R. T. Lahey and F. J. Moody, *The Thermal-hydraulics of a Boiling Water Nuclear Reactor*. American Nuclear Society, 1993.

[9] S. Sugawara, "Droplet deposition and entrainment modeling based on the three-fluid model," *Nuclear Engineering and Design*, vol. 122, no. 1-3, pp. 67-84, Sep. 1990.

[10] S. Jayanti and M. Valette, "Prediction of dryout and post-dryout heat transfer at high pressures using a one-dimensional three-fluid model," *International Journal of Heat and Mass Transfer*, vol. 47, no. 22, pp. 4895-4910, 2004.

[11] N. Hoyer, "Calculation of dryout and post-dryout heat transfer for tube geometry," *International Journal of Multiphase Flow*, vol. 24, no. 2, pp. 319-334, Mar. 1998.

[12] R. J. Belt, J. M. C. Van't Westende, and L. M. Portela, "Prediction of the interfacial shear-stress in vertical annular flow," *International Journal of Multiphase Flow*, vol. 35, no. 7, pp. 689-697, Jul. 2009.

[13] A. G. B. Wallis, *One-dimensional Two-phase Flow*. McGraw-Hill, 1969.

[14] T. Okawa, A. Kotani, I. Kataoka, and M. Naitoh, "Prediction of the critical heat flux in annular regime in various vertical channels," *Nuclear Engineering and Design*, vol. 229, no. 2-3, pp. 223-236, Apr. 2004.

[15] G. F. Hewitt and A. H. Govan, "Phenomenological modelling of non-equilibrium flows with phase change," *International Journal of Heat and Mass Transfer*, vol. 33, no. 2, pp. 229-242, Feb. 1990.

[16] C. Adamsson, *Dryout and power distribution effects in boiling water reactors*.: Thesis, School of Engineering Sciences, Royal Institute of Technology, 2009.

[17] Stewart, C.W et al., *VIPRE-01: A thermal-hydraulic code for reactor cores*. 1989.

[18] K. Brynjell-Rahkola, J.-M. Le Corre, and C. Adamsson, "Validation of VIPRE-W Sub-channel Void Predictions using NUPEC/BFBT Measurements," in *The 13th International Topical Meeting on Nuclear Reactor Thermal Hydraulics (NURETH-13)*, 2009.

[19] J.-M. Le Corre and C. Adamsson, "Development of a New Mechanistic Tool for the Prediction of the Liquid Film Dryout during a Transient," in *The 13th International Topical Meeting on Nuclear Reactor Thermal Hydraulics (NURETH-13)*, 2009.

[20] D. Moxon and P. A. Edwards, *Dryout during flow and power transients*. 1967.

[21] C. Adamsson and J.-M. Le Corre, "On a best-estimate approach to the calculation of dryout probability during BWR," in *The 14th International Topical Meeting on Nuclear Reactor Thermal Hydraulics (NURETH-14)*, 2011.

[22] B. Neykov, F. Aydogan, L. Hochreiter, and K. Ivanov, *NUPEC BWR Full-size Fine-mesh Bundle Test (BFBT) Benchmark, Vol. I: Specifications*. 2006.

[23] J.-M. Le Corre, C. Adamsson, and P. Alvarez, "Transient void, pressure drop and critical power BFBT benchmark analysis and results with VIPRE-W/MEFISTO-T," in *The 14th International Topical Meeting on Nuclear Reactor Thermal Hydraulics (NURETH-14)*, 2011.